Research Article

Mohammad Reza Karimzadeh, Sara Soltanian*, Mahboubeh Sheikhbahaei, and Neda Mohamadi

Characterization and biological activities of synthesized zinc oxide nanoparticles using the extract of *Acantholimon serotinum*

https://doi.org/10.1515/gps-2020-0058
received June 23, 2020; accepted September 27, 2020

Abstract: The present study reports the synthesis of ZnO-NPs using *Acantholimon serotinum* extracts followed by characterization and evaluation of biological activities. Field emission scanning electron microscope revealed irregular spherical morphology with a size in the range of 20–80 nm. The X-ray diffraction analysis confirmed the synthesis of highly pure ZnO NPs with a hexagonal shape and a crystalline size of 16.3 nm. The UV-Vis spectroscopy indicates the synthesis of ZnO-NPs. FT-IR confirmed the presence of phytocomponents in the plant extract, which was responsible for nanoparticle synthesis. According to MTT results, the biosynthesized ZnO-NPs showed cytotoxic effects on human colon cancer Caco-2 (IC_{50}: 61 μg/mL), neuroblastoma SH-SY5Y (IC_{50}: 42 μg/mL), breast cancer MDA-MB-231 (IC_{50}: 24 μg/mL), and embryonic kidney HEK-293 (IC_{50}: 60 μg/mL) cell lines. Significant reactive oxygen species (ROS) generation was measured by the DCFH-DA assay after 24 h incubation with ZnO-NPs (200 μg/mL). ZnO-NPs caused apoptotic and necrotic effects on cells, which was confirmed by Annexin V-PE/7-AAD staining and 6.8-fold increase in pro-apoptosis gene Bax and 178-fold decrease in anti-apoptosis gene Bcl-2. The well diffusion method did not show effective growth inhibition activities of the ZnO-NPs against bacteria. In conclusion, the ZnO-NPs induce cytotoxicity in cell lines through ROS generation and oxidative stress.

*** Corresponding author: Sara Soltanian,** Department of Biology, Faculty of Science, Shahid Bahonar University of Kerman, Kerman, Iran, e-mail: Soltanian@uk.ac.ir, sarasoltanian@gmail.com, tel: +98-34-31-32-2068; fax: +98-34-33-25-7432
Mohammad Reza Karimzadeh: Department of Medical Genetics, School of Medicine, Bam University of Medical Sciences, Bam, Iran
Mahboubeh Sheikhbahaei: Department of Biology, Faculty of Science, Shahid Bahonar University of Kerman, Kerman, Iran
Neda Mohamadi: Herbal and Traditional Medicines Research Center, Department of Pharmacogenosy, Kerman University of Medical Sciences, Kerman, Iran

Keywords: zinc oxide nanoparticles, *Acantholimon serotinum*, cytotoxicity, anti-bacterial activity, oxidative stress

Abbreviations

DCF	2,7-dichlorofluorescein
DCFH-DA	2,7-dichlorofluorescein diacetate
FTIR	Fourier-transform infrared spectroscopy
MTT	3-(4,5-dimethyl-2-thiazolyl)-2,5-diphenyl-2H-tetrazolium bromide
NPs	nanoparticles
PS	phosphatidylserine
ROS	reactive oxygen species
SEM	scanning electron microscopy
ZnO-NPs	zinc oxide nanoparticles

1 Introduction

Nanoparticles (NPs) have been introduced in many fields of biology, medicine, and material science and have been harnessed for application in diverse fields such as tissue engineering, drug design, and gene therapy to develop new therapeutic approaches over the last decade [1–3]. Metal NPs research has recently received special attention due to their unusual properties when compared with bulk metal [4]. For example, zinc oxide nanoparticles (ZnO-NPs) have become one of the most popular metal oxide NPs in industrial, pharmaceutical, and biological applications [5]. Physical and chemical methods that are used for the synthesis of metal NPs such as ZnO-NPs are expensive and toxic. Green biosynthesis of ZnO-NPs is the use of reducing and capping agents obtained from plant material that eliminates the use of noxious chemicals with toxic effects [6,7]. Furthermore, many scientists have been attracted to use such resources for the biosynthesis of metal NPs due to the ease of production, diversity in size and

shape, and enhanced biocompatibility of NPs relative to other methods. Until now, green synthesis of ZnO-NPs using different plant extracts and their potential applications in biology were reported [8,9]

Acantholimon Boiss is a genus in the family Plumbaginaceae composed of approximately 200 species that most of them are distributed in Irano-Turanian phytogeographic region [10–13]. It was shown that plants from the Plumbaginaceous family contain secondary metabolites including plumbagin, lignin, saponins, anthocyanin, quinines, alkaloids, simple phenolic, tannins, and flavonoids that are responsible for their biological effects [14,15]. Until now, little attention has been given to the identification of phytochemicals and biological activities of the genus *Acantholimon* [16]. Recently, cytotoxic, antioxidant, and antibacterial activities of three species of *Acantholimon* including *A. austro-iranicum, A. serotinum* and *A. chlorostegium* were investigated by Soltanian et al. [17].

In this study, ZnO-NPs were green synthesized using *A. serotinum* methanol extract for the first time. Synthesized ZnO-NPs were characterized by various techniques, and cytotoxic activity against several types of cancer and normal cell lines and antibacterial activity against two gram-positive (*Enterococcus faecalis* and *Staphylococcus aureus*) and two gram-negative (*Pseudomonas aeruginosa* and *Escherichia coli*) bacteria were evaluated. In addition, this study showed that the exposure of cells to ZnO-NPs leads to reactive oxygen species (ROS) generation, upregulation of Bax and downregulation of Bcl-2, and finally apoptosis/necrosis induction.

2 Materials and methods

2.1 Plant extraction procedure

Aerial parts of *Acantholimon serotinum* Rech.f.& Schiman-Czeika were collected from Baft to Khabr, Kerman Province, Southeast of Iran, identified according to the standard keys, and deposited in MIR herbarium under voucher number 1968. Dry powdered plant material was extracted using a maceration technique with methanol 80% and then dried in the oven (Vacucell, Einrichtungen GmbH) at 40°C [17–19].

2.2 Biosynthesis of ZnO-NPs

The amount of 10 mL of plant extracts sample (100 µg/mL in distilled water) was added to 100 mL of 0.1 M zinc sulfate ($ZnSO_4$) aqueous solution. An aqueous solution of NaOH was gradually added into the solution under the steady stirring until the pH of the solution reached to 8 to attain smaller size particles [20]. The solution was kept on a magnetic stirrer at 60°C for 6 h. The yellowish-brown color of the solution indicated the formation of the particles. The solution was centrifuged at 10,000 rpm for 10 min, the supernatant was discarded, and the pellet was washed using deionized water 4–5 times; afterward, it was washed by ethanol around 3 times to remove organic impurities. After washing, the samples were dried in an oven at 50°C.

2.3 Characterizations of ZnO-NPs

The formation of ZnO-NPs was monitored using a UV-Vis spectrophotometer (PerkinElmer, Germany) at 300–600 nm. Field emission scanning electron microscopy (FESEM) (Quanta 200, USA) was used for examination of the size, morphology, and distribution of synthesized samples. Crystallographic properties of ZnO NPs were explored using the X-ray diffraction (XRD) technique within $2\theta = 10–90$ using the XRD instrument (Rigaku, Ultima IV, Tokyo, Japan) with a Cu LFF $\lambda = 1.540598$ A as a radiation source. The obtained pattern from the XRD was then analyzed using X'Pert High Score Plus software, and the chemical composition, crystalline structure, and size of the NP were identified. The size of the particles was calculated using the Debye–Scherrer equation:

$$D = 0.9\lambda/\beta \cos\theta \quad (1)$$

where D is the crystalline size, λ is the wavelength of X-ray used, β is the full line width at the half maximum (FWHM) elevation of the main intensity peak, and θ is the Bragg's angle.

The NPs and plant extract were subjected to Fourier transform infrared spectra (FT-IR) spectrometric analysis to specify the functional groups in the extract that may be responsible for reducing ions to NPs.

2.4 Cell culture and cytotoxic activity

To examine the cytotoxic activity of ZnO-NPs, human colon cancer (Caco-2), neuroblastoma (SH-SY5Y), breast cancer (MDA-MB-231), and embryonic kidney (HEK-293) cell lines were cultured with Dulbecco's Modified Eagle's Medium (DMEM) supplemented with 10% fetal bovine serum (FBS), 100 µg/mL penicillin and 100 µg/mL streptomycin and incubated at 37°C (5% CO_2). The attached cells were trypsinized for 3–5 min to get the individual cells. The cells were counted and distributed in a 96-well

plate with 5,000 cells in each well. The plate was incubated for 24 h to allow the cells to form ~70–80% confluence as a monolayer. Cytotoxicity of ZnO-NPs was determined by 3-(4,5-dimethylthiazol-2-yl)-2,5-diphenyltetrazolium bromide (MTT) assay. For this, cells were exposed for 48 h to different concentrations (10, 20, 40, 80, 160, 320, and 640 µg/mL) of ZnO-NPs. To detect the cell viability, 20 µL MTT solution was added to each well and incubated for 3 h. Then, the MTT solution was removed and 100 µL DMSO was added to each well followed by 15 min incubation. The optical density of the formazan product was taken at 499 nm in a microplate reader (BioTek-ELx800, USA), and the percentage of cell viability was calculated as follows: $A_{\text{treatment}}/A_{\text{control}} \times 100\%$ (where, A = absorbance). The mean of three absorbance values were calculated for each concentration. The date was used to determine IC_{50} value, a concentration that a cytotoxic agent induces a 50% growth inhibition [21].

2.5 Intracellular ROS detection

The level of intracellular ROS was assessed by measuring the oxidation of 2′,7′-dichlorodihydrofluorescein diacetate (DCFH-DA). DCFH-DA diffuses through the cell membrane and is deacetylated by cellular esterase to the non-fluorescent DCFH. Intracellular ROS can oxidize DCFH to the fluorescent 2,7-dichlorofluorescein (DCF); therefore, the intensity of fluorescence is directly proportional to the levels of intracellular ROS [22,23]. Briefly, 25×10^3 cells were cultured in 96-well microplates. After 24 h, the medium was removed and replaced by a medium containing 10 µM of DCFH-DA (Sigma-Aldrich, Germany), and cells were kept in a humidified atmosphere (5% CO_2, 37°C) for 45 min. To measure intracellular ROS, cells were exposed to various concentrations of ZnO-NPs (25–200 µg/mL) or 600 µM H_2O_2 as a positive control. After 3 and 24 h, fluorescence was measured at an excitation wavelength of 485 nm and an emission wavelength of 538 nm (FLX 800; BioTek). Results were expressed as the percentage of fluorescence intensity relative to untreated control cells [23,24].

2.6 *In vitro* apoptosis/necrosis assay

PE-conjugated-Annexin V/7-AAD assay (BD Biosciences kit) was used to quantitatively determine the percentage of cells within a population that are actively undergoing apoptosis/necrosis. At >90% confluence, the HEK-293 cells (4×10^5 cells/6 cm dish) were incubated with prepared ZnO-NPs at 60 µg/mL concentration. Untreated HEK-293 cells were used as a negative control. Following treatment for 48 h, both adherent and floating cells were collected and washed with PBS. The cell pellets were suspended in 100 µL Annexin V binding buffer, 5 µL PE-Annexin V, and 5 µL 7-AAD. The tube was gently vortexed and incubated for 15 min in dark condition. Following the addition of 400 µL binding buffer, the samples were used for flow cytometric analysis by BD FACS Calibur™ (BD Biosciences, San Jose, CA, USA) at an excitation wavelength of 488 nm. PE was detected in fluorescence channel 2 (FL2): 575/30 band pass filter (BP) and 7-AAD were detected in channel 3 (FL3): 620/30 BP [25,26].

2.7 Analysis of apoptosis-related gene expression

An SYBR Green real-time quantitative PCR was carried out to compare the expression levels of Bax and Bcl-2 mRNAs in untreated and ZnO-NPs-treated HEK-293 cells. HEK-293 cells were seeded into 6 cm dishes (5×10^4 cells/well) and incubated for 24 h, then the cells were treated with 60 µg/mL ZnO-NPs for 48 h. Total cellular RNA was extracted from cells using the total RNA isolation kit (DENAzist Asia, Mashhad, Iran) according to the manufacturer's instructions. The quantity and quality of RNA were assessed using a Nanodrop and agarose gel electrophoresis. The cDNA was synthesized using M-MuLV reverse transcriptase (Cat. No. EP0441; Thermo Scientific, Wilmington, USA), according to protocol. The primers used for real-time PCR were as follows: forward 5′-CCCG AGAGGTCTTTTTCCGAG-3′ and reverse 5′- CCAGCCCATGA TGGTTCTGAT-3′ for Bax, and forward 5′-CATGTGTGTGG AGAGCGTCAA-3′ and reverse 5′-GCCGGTTCAGGTACTCAG TCA-3′ for Bcl-2. Also, the sequence of the forward primer for the internal control gene beta-2-microglobulin (β2M) was 5′-CTCCGTGGCCTTAGCTGTG-3′ and that of the reverse primer was 5′-TTTGGAGTACGCTGGATAGCCT-3′.

The expression of the target genes was studied using an Analytik Jena, a real-time PCR system (Germany). Each PCR amplification reaction was performed in 20 µL reaction mixture containing 10 µL of 2× SYBR Green master mix (Cat. No. 5000850-1250; Amplicon, UK), 0.5 µL of each

primer (0.25 µM), 1 µL cDNA (50 ng), and 8 µL double-distilled water. After denaturation at 95°C for 15 min, 40 cycles were followed by 95°C for 15 s, 60°C for 20 s, and 72°C for 10 s in PCR cycling condition. The amplification stage was followed by a melting stage that temperature was increased in steps of 1°C for 10 s from 61°C to 95°C.

A comparative threshold cycle method was used to determine the relative expression level of the target gene. For this, the mean threshold cycle value of β2M as a reference gene was subtracted from the mean threshold cycle value of the target genes (Bax and Bcl-2) to obtain ΔCT and fold change in the target gene of ZnO-NPs-treated cell relative to the untreated control sample was calculated according to the following equation: Fold change = $2^{(-\Delta\Delta CT)}$ where ΔΔCT is calculated by the following equation: $\Delta CT_{\text{test sample}} - \Delta CT_{\text{control sample}}$ [27,28].

2.8 Determination of antibacterial property

The antibacterial potential of synthesized ZnO-NPs was tested against *Enterococcus faecalis* (ATCC 29212), *Staphylococcus aureus* (ATCC 25838), *Pseudomonas aeruginosa* (ATCC 27853), and *Escherichia coli* (ATCC 11333) bacteria using the agar well diffusion method. Briefly, the Muller Hinton agar plates were inoculated with 1 mL (10^8 colony-forming units) of bacterial cultures using spread-plating. After drying the plates, wells of size 6 mm have been made on Muller–Hinton agar plates using gel puncture. 100 µL of various concentrations (500, 1,000, 3,000 µg/mL) of ZnO-NPs was poured in each well. The culture plates were incubated at 37°C for 24 h. After the growth period, the plates were removed and the antibacterial activity was measured based on the inhibition zone (millimeters) around wells poured with the nanoparticle. Ciprofloxacin (25 mg/mL) and deionized water were used as a positive and negative control, respectively. The experiment was repeated three times [29,30].

2.9 Statistical analysis

The one-way analysis of variance (ANOVA) was used to determine whether there are any statistically significant differences between the means of control and treatments. The data were shown as mean ± SD and $p < 0.05$ accepted as the minimum level of significance.

3 Results

3.1 Characterizations of ZnO-NPs

UV-Vis spectra showed a strong peak at 380 nm confirming the ZnO-NPs synthesis (Figure 1a).

The size of sphere-like shaped ZnO-NPs was measured in the range of 20–80 nm using the FESEM image (Figure 1b). The crystalline structure of the ZnO NPs revealed the presence of distinct line broadening of XRD peaks with no remarkable shift in the diffraction peaks indicating that the crystalline product was without any impurities. The XRD peaks were observed at 31.76°, 34.42°, 36.25°, 47.51°, 56.59°, 62.85°, 66.37°, 67.94°, 69.08°, 72.5°, 76.9°, 81.3°, and 89.63°, which are indexed in crystal system of hexagonal phase with a space group of *P*63*mc* and reference code of 01-079-0206. The findings are in accordance with the results of Mahendra et al. that they reported the green synthesis of ZnO-NPs of *Cochlospermum religiosum* was without any impurities in the crystalline product [8]. The crystalline size of the bio-synthesized ZnO NPs was found to be about 16.3 nm from the FWHM of the most intense peak corresponding to 101 plane located at 36.25° using Debye–Scherrer equation (Figure 1c). The FT-IR was analyzed in the range of 0–4,000 cm^{-1} to recognize the various functional groups present in the synthesized NPs and plant extract. In the case of AgNPs, the intense absorption band at 3406.23 cm^{-1} was occurred due to O–H which was related to the adsorption of water on the surface of ZnO-NPs. The intense peaks at 2853.86 and 2923.61 cm^{-1} indicate the presence of C–H stretch. Bands at 1362.71 cm^{-1} assigned to –C–H bending vibrations absorption bands 1048.81 and 1126.02 cm^{-1} indicate the significant presence of C–O stretch which is a functional group of alcohols, carboxylic acids esters, and ethers. The absorption at 600 cm^{-1} indicates the presence of ZnO-NPs. FT-IR results for Plant extract showed a broad range at 3411.42 corresponding to O–H stretch, H-bonded in alcohols, and phenols. Weak peaks obtained at 2931.61 depicted the presence of C–H stretch alkane group. The band at 1617.59 cm^{-1} in plant extract was due to the presence of and C–C stretch (in–ring), C–N stretch of amide I in proteins or C═O stretch in polyphenols which was shifted to 1699.59 cm^{-1} in ZnNPs due to the proteins or polyphenols that may have been linked to NPs by the amine or phenolic groups. Medium peaks obtained at 1448.60 and 1040 cm^{-1} illustrated C–H bend alkanes group. Weak bonds obtained at 650–1,000 cm^{-1} represented ═C–H bend alkenes group (Figure 1d) [31].

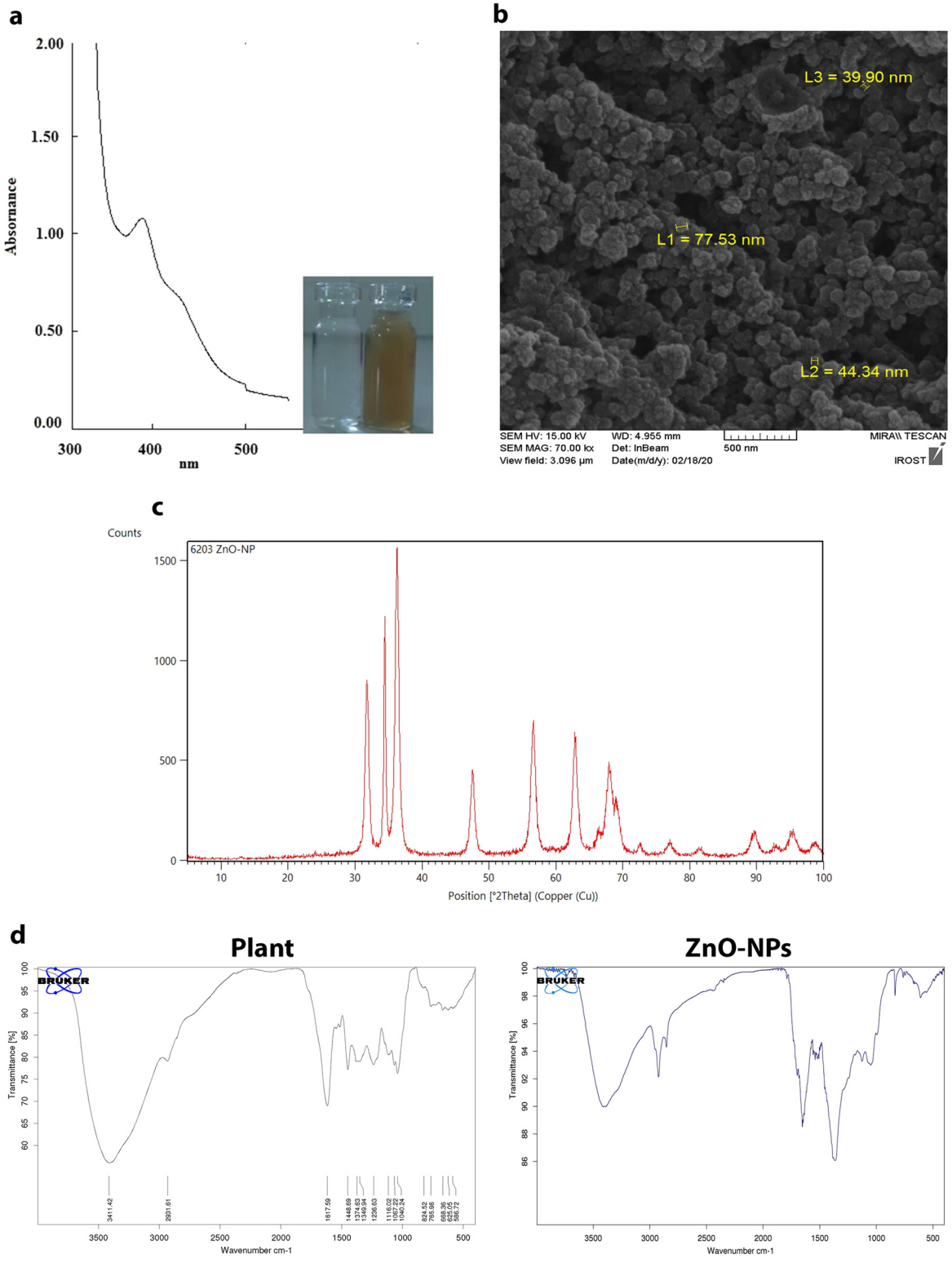

Figure 1: Characterization of green synthesized ZnO-NPs prepared using methanol extract of the *A. serotinum* plant. The UV-Vis spectrum of ZnO-NPs synthesized by *A. serotinum* and color change of zinc sulfate to ZnO-NPs (a), FESEM image (b), X-ray powder diffraction pattern of the green synthesized ZnO-NPs (c) and FT-IR spectrum for plant extract and synthesized ZnO-NPs (d).

3.2 Determination of cytotoxic effect of synthesized ZnO-NPs

MTT is a colorimetric assay based on the mitochondrial succinate dehydrogenase activity of viable cells [32]. MTT assay was performed to investigate the *in vitro* cytotoxic property of ZnO-NPs. Caco-2, SH-SY5Y, MDA-MB-231, and HEK-293 cell lines were treated with different concentrations of synthesized ZnO-NPs for 48 h to determine the inhibitory percentage. Based on the results, cell viability was proportional to the concentration of the ZnO-NPs. ZnO-NPs showed very potent cytotoxic activity in a way that the viability of Caco-2, SH-SY5Y, MDA-MB-231, and HEK-293 cell lines decreased by 50% following 48 h of incubation with 61, 42, 24, and 60 µg/mL concentration of ZnO-NPs, respectively. The obtained concentrations values corresponding to a survival rate of 50% is defined as the IC_{50} values for each cell lines (Figure 2).

3.3 Determination of intracellular ROS

Results obtained from ROS generation in HEK-293 cells exposed to H_2O_2 (600 µM) and different concentrations of ZnO-NPs (25, 50, 200 µg/mL) for 3 and 24 h are shown in Figure 3. A statistically significant induction in ROS generation was measured in HEK-293 cells exposed to H_2O_2 as a positive control for oxidative stress. Cells that were treated with ZnO-NPs for 3 h did not increase ROS as compared to untreated control (Figure 3a). However, the ROS level increased 2-fold after exposure to 200 µg/mL ZnO-NPs for 24 h when compared to control cells (Figure 3b).

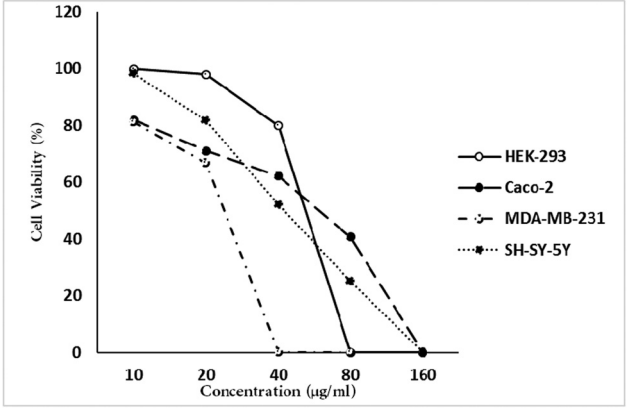

Figure 2: Anti-proliferative activity of ZnO-NPs. SH-SY5Y, HEK 293, Caco-2, and MDA-MD-231 cell lines were treated with different concentrations of ZnO-NPs (5, 10, 20, 40, 80, 160, 320, 640 µg/mL) for 48 h and subjected to MTT assay and cell viability was calculated.

3.4 Apoptosis/necrosis assessment using annexin V-PE and 7-AAD

Annexin-V/7-AAD detection kit takes advantage of the fact that phosphatidyl serine (PS) translocate from the inner (cytoplasmic) leaflet of the plasma membrane to the outer (cell surface) leaflet soon after the induction of apoptosis and that the Annexin V protein has a strong, specific

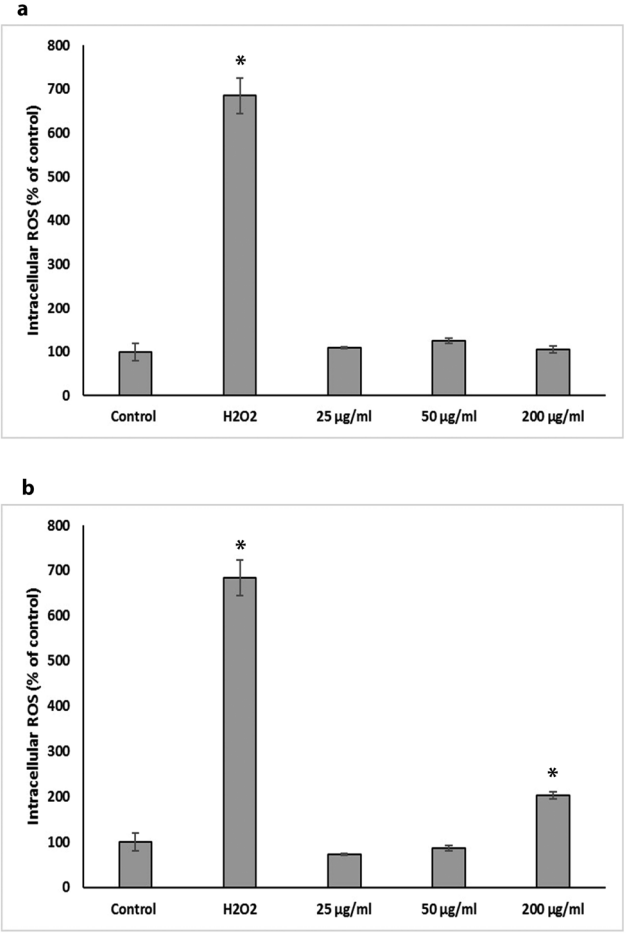

Figure 3: Evaluation of ROS generation in HEK-293 cells using the fluorescent probe DCF. Cells were treated with different concentrations of ZnO-NPs (25, 50, 200 µM) and positive control (600 µM H_2O_2) for 3 h (a) and 24 h (b). Data are expressed as a percent of values of untreated control cells and are means ± SD of three independent experiments. * indicates a statistically significant difference from corresponding untreated control cells ($p < 0.05$).

affinity for PS [33]. Moreover, late apoptotic cells and necrotic cells lose their cell membrane integrity and are permeable to vital dyes such as 7-AAD [34]. Hence, the annexin $V^{+}/7\text{-}AAD^{-}$ cells detect early stage of apoptosis, annexin V^{+}/PI^{+} cells exhibit late stage of apoptosis, annexin V-/7-AAD+ cells represent necrosis, and annexin $V^{-}/7\text{-}AAD^{-}$ cells show live cells. Flow cytometric analysis of Annexin V-PE staining showed 96% of HEK-293 control cells were alive. There are about 25% and 14% increases in late apoptotic and necrotic cell population in HEK-293 cells treated with ZnO-NPs, respectively, as compared with untreated ones (Figure 4).

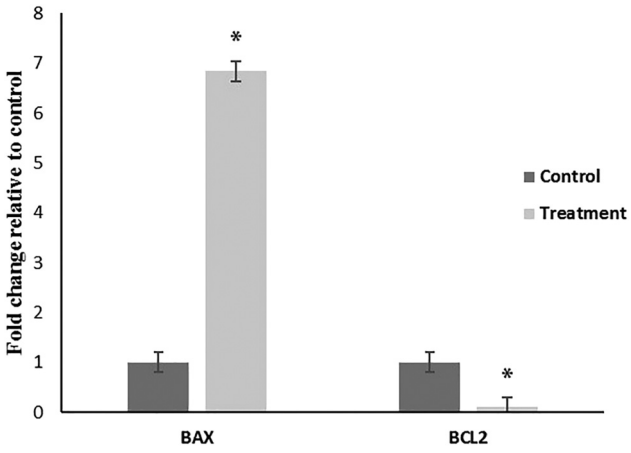

Figure 5: Gene expression ratio of Bcl-2 and Bax in HEK-293 cells exposed to ZnO-NPs compared to untreated control cells. HEK-293 cells were treated with ZnO-NPs (60 µg/mL) for 48 h. Expression of Bax and Bcl-2 were considered as 1 in untreated control HEK-293 cells and the level of genes after treatment with ZnO-NPs are represented as the fold change over the untreated controls.

3.5 Analysis of apoptosis-related gene expression

In this study, the expression of pro-apoptotic and anti-apoptotic genes at the mRNA level in ZnO-NPs-exposed HEK-293 cell line was studied using quantitative real-time PCR (Figure 5). Our findings show that the mRNA level of *Bax* was significantly upregulated (6.8-fold), while the expression of the *Bcl-2* was significantly diminished (178-fold) in cells treated with ZnO-NPs when compared with normal cells. These results confirm that the exposure of ZnO-NPs induced substantial apoptosis in HEK-293 cells.

3.6 Antibacterial activity

Owing to bacterial resistant to antibiotics and metal ions, scientists have focused on using NPs for killing the pathogenic bacteria [35]. In this report, the anti-microbial activity of synthesized ZnO-NPs against four bacteria strains was studied by the agar well diffusion method and results are given in Table 1. According to the zone of inhibition, ciprofloxacin showed good inhibitory activity for all the

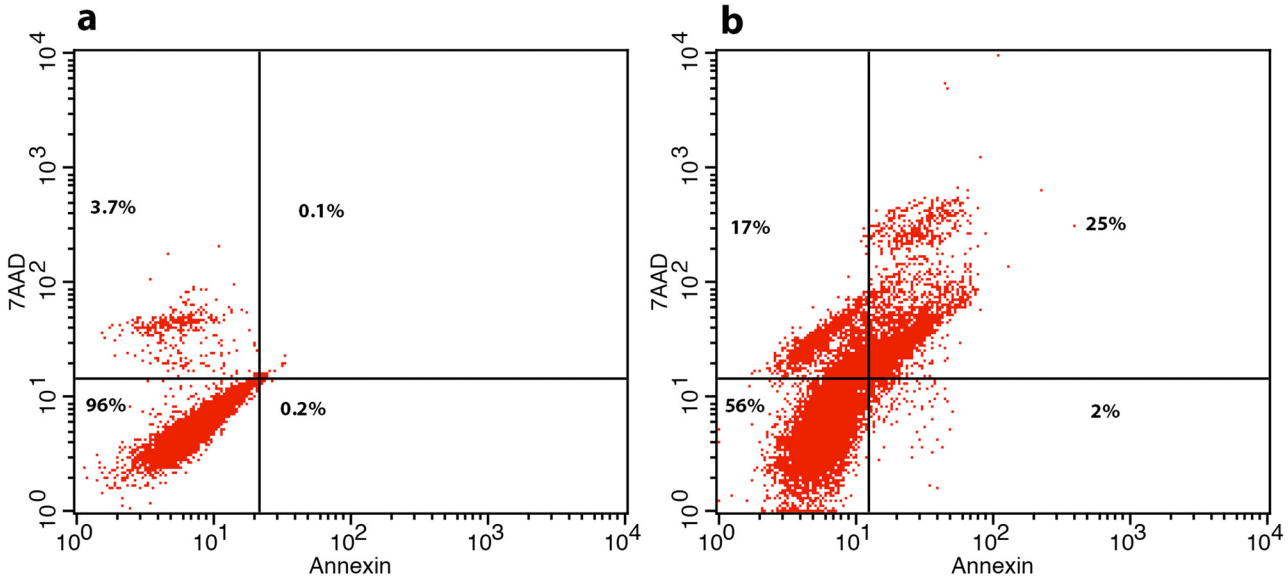

Figure 4: Flow cytometric analysis of ZnO-NPs -induced HEK-293 cells apoptosis. Flow cytometry dot plots of Annexin V-FITC/7-AAD double staining of control HEK-293 cells without treatment (a) and after treatment with ZnO-NPs (b).

Table 1: Well diffusion method for analysis of the antibacterial activity of ZnO-NPs against four bacteria strains and ciprofloxacin is used as a positive control

Zone of inhibition (mm ± SD) against bacteria strains				
ZnO-NPs concentration (µg/mL)	***Pseudomonas aeruginosa***	***Escherichia coli***	***Enterococcus faecalis***	***Staphylococcus aureus***
500	—	—	—	—
1,000	—	—	—	—
3,000	3	5	3	5
Ciprofloxacin (25,000)	40	39	41	39

tested bacterial strains and synthesized ZnO-NPs showed weak antibacterial activities. About 3,000 µg/mL was recorded as the lowest concentration at which antibacterial activities on two Gram-positive strains: *E. faecalis* and *S. aureus* and two Gram-negative strains: *P. aeruginosa* and *E. coli* were demonstrated. We found no antibacterial activity at a lower concentration of ZnO-NPs.

4 Discussion

Plants have some biomolecules and bio-reducing agents such as enzymes, proteins, flavonoids, terpenoids, and cofactors that provide a versatile, economical, and eco-friendly method to fabricate metal NPs. ZnO-NPs synthesis using whole-plant extract is reported in number of plants [8,9,30,36–44].

The bioreduction of ZnO-NPs using methanol extracts of *A. serotinum* was investigated in this study. Synthesized ZnO-NPs were characterized using UV-Vis spectroscopy, FT-IR, and FESEM. UV-Vis spectra suggested the presence of a strong peak at 380 nm confirming the NPs synthesis. FESEM micrograph demonstrated the presence of spherical NPs with a size range of 20–80 nm. FT-IR confirmed the presence of some functional groups such as free hydroxyl, aromatic, carbonyl, primary amine, and carboxylic acid in the plant extract which were responsible for nanoparticle synthesis. FT-IR revealed that proteins or other soluble organic compounds in the extract may bind with zinc ions and reduce the zinc ions to NPs. After characterization, cytotoxicity, ROS production, induction of apoptosis and necrosis and antibacterial activities of green bio-synthesized ZnO-NPs were investigated in this study. The evaluation of the antiproliferative/cytotoxic activity against human colon carcinoma (Caco-2), neuroblastoma (SH-SY5Y), breast (MDA-MB-231), and embryonic kidney (HEK-293) cells showed the great cytotoxic potential of green ZnO-NPs with IC_{50} value of 61, 42, 24, and 60 µg/mL. In our previous research, the cytotoxicity of methanol extract of *A. serotinum* was tested on various cancer cell lines [17]. When the IC_{50} of the ZnO-NPs and extract were compared, the cytotoxic potential of synthesized ZnO-NPs was higher than the *A. serotinum* extract (IC_{50} values of extract for neuroblastoma, breast, and colon cancer cell lines were calculated as 328, 403, and 600 µg/mL) [17]. It might be due to the synergetic effects of biomolecular groups derived from *A. serotinum* that adhered to the process of ZnO-NPs synthesis [45]. Moreover, nanosized particles may improve their stability and cell penetration leading to enhanced bioavailability and cytotoxicity [46]. As a result, cytotoxic effects induced by ZnO-NPs can be attributed to both nanosized zinc and bioactive phytocompounds attached on the surface of ZnO-NPs [46]. This is the first investigation to introduce the cytotoxicity of photosynthesized ZnO-NPs using methanol extract of *A. serotinum* against cancer and normal cell lines. Cytotoxicity and anticancer effects of biosynthesized ZnO-NPs using another plant extracts such as *Punica granatum*, *Silybum marianum*, *Tectona grandis*, *Tamarindus indica*, *Nepeta deflersiana*, and *Albizia lebbeck* also supported results obtained from this study [9,24,30,39,40,47]. Unfortunately, these findings suggest that the *A. serotinum* ZnO-NPs did not show specificity and selectivity toward the cancerous cells when compared with the normal cells; therefore, it is not selective enough to be useful as an anticancer compound. Moreover, we demonstrated that synthesized ZnO-NPs induce the generation of ROS in cells. Our results are in good agreement with the recent reports that have shown NPs such as ZnO-NPs can stimulate ROS formation [24,48–50]. Therefore, it is approved that the toxicity of ZnO-NPs is induced by the generation of ROS. Free radicals generated by ZnO-NPs would oxide and modify macromolecules including proteins, enzymes, membrane lipids, and DNA which subsequently result in oxidative damage of organelles and cell apoptosis. Staining the cells with Annexin V and 7-AAD solution showed that the cytotoxicity of ZnO-NPs toward HEK-293 cells was mediated by apoptosis and necrosis induction. In other reports, apoptotic and necrosis

induction was also observed after exposure of cells to plant-synthesized ZnO-NPs [48,50–52].

Further studies to illuminate the ZnO-NP-induced apoptosis was conducted by expression analysis of *Bax* and *Bcl-2*. The BCL-2 protein family consisting of anti-apoptotic and pro-apoptotic members acts as a critical life-death decision point within the common pathway of apoptosis. BCL-2 as an anti-apoptotic member of this family prevents apoptosis. In contrast, pro-apoptotic members of this family, such as BAX lead to caspase activation and trigger apoptosis [53]. Real-time PCR results showed that the expression of pro-apoptotic *Bax* gene was significantly upregulated, while the expression of the anti-apoptotic *Bcl-2* gene was significantly reduced in cells treated with ZnO-NPs when compared with normal cells. In accordance with our results, previous researches also showed the upregulation of *Bax* and downregulation of *Bcl-2* during apoptosis induction by NPs such as ZnO-NPs [27,28]. Figure 6 shows the mechanism of the toxicity of ZnO-NPs.

Owing to bacteria resistance to antibiotic and metal ions, scientists have focused on the development of other methods such as NPs for killing the pathogenic bacteria [35]. Photosynthesized ZnO-NPs in this research showed weak antibacterial activity.

It has been reported that NPs interact with the bacterial cell wall or membrane and release metal ions that result in the disruption of the cell permeability and production of ROS inside the cell. This can damage DNA and denature proteins that finally trigger apoptosis or cell death [42]. Antibacterial activities of ZnO-NPs depend on morphology, particle size, powder concentration, specific surface area, etc. [30]. For example, smaller NPs having a large surface area available for interaction have more antibacterial effect than the larger nanoparticle. On the other hand, it is demonstrated that when the concentration of plant extract increase, antimicrobial activities of green synthesized NPs increase because the presence of the plant extract on the surface of the NPs enhance nanoparticle solubility. An increase in solubility leads to permeation of NPs through the bacterial cell wall, disturbance in cell metabolism, and finally cell death [29]. Since properties of ZnO-NPs and synthesis condition can affect on antibacterial properties, biosynthesized ZnO-NPs with various plant extracts such as *Cassia alata, Tectona grandis, Cochlospermum religiosum, Albizia lebbeck, Punica granatum*, and *Silybum marianum* showed different antibacterial activities [8,9,30,39–41,54]. Weak antimicrobial activity of ZnO-NPs that was seen in our results may be due to agglomeration of ZnO-NPs in the solution using van der Waals forces and superficial effects [55,56].

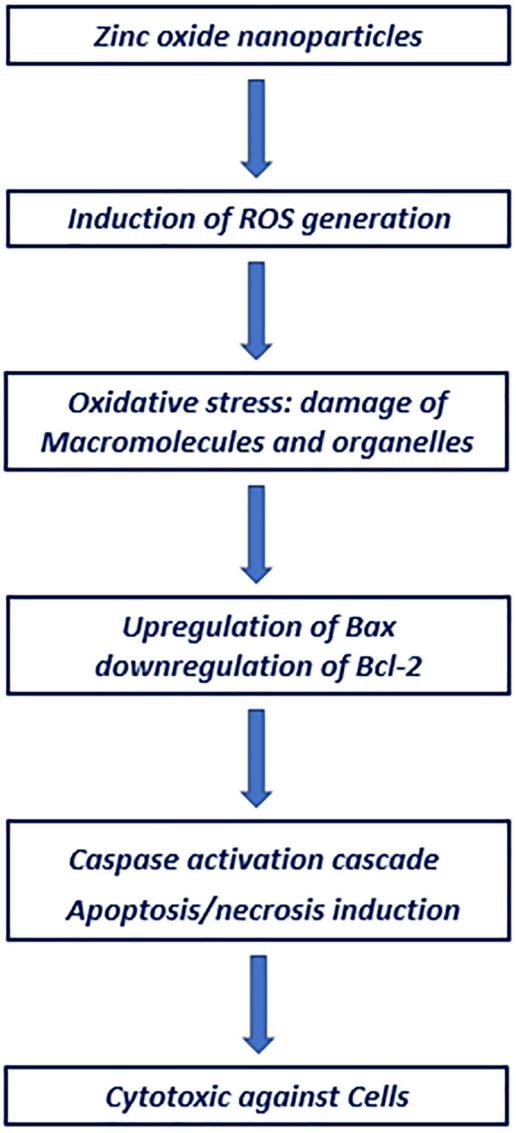

Figure 6: Mechanism of toxicity of ZnO-NPs against cell lines.

In conclusion, plants have some biomolecules and bioreducing agents such as enzymes, proteins, flavonoids, terpenoids, and cofactors that provide a versatile, economical, and eco-friendly method to fabricate metal NPs [57,58]. ZnO-NPs synthesized with natural plant extracts have broad applications in the biomedical and industrial fields. In this study, ZnO-NPs were synthesized using a methanol extract of *A. serotinum* for the first time. The synthesized NPs exhibited potential cytotoxic activities against cancer and normal cell lines. The production of ROS analyzed using DCFH-DA assay is an essential mechanism through which ZnO-NPs induce oxidative stress and apoptosis. 7-AAD and Annexin-V dyes demonstrated that ZnO-NPs have the potential to induce apoptosis and necrosis. Apoptosis induction was further evaluated by

expression analysis of two important members of BCL-2 family including *Bax* and *Bcl-2*. The antibacterial activity of the ZnO-NPs was examined on four bacterial stains, and it was discovered that ZnO-NPs synthesized by *A. serotinum* have weak antibacterial activity. Hence, it is concluded that the synthesized ZnO-NPs show cytotoxicity by the generation of ROS, leading to oxidative stress and eventually cell death.

Acknowledgments: This work was supported by the Bam University of Medical Science, Bam, Iran, under Grant [number 98000048]. The authors thank Dr. Mansour Mirtadzadini at the Department of Biology, Faculty of science, Shahid Bahonar University of Kerman for plant collection and identification.

Conflict of interest: The authors declare no conflict of interest.

References

[1] Hackenberg S, Scherzed A, Kessler M, Hummel S, Technau A, Froelich K, et al. Silver nanoparticles: evaluation of DNA damage, toxicity and functional impairment in human mesenchymal stem cells. Toxicol Lett. 2011;201:27–33.

[2] Yokoyama K, Welchons D. The conjugation of amyloid beta protein on the gold colloidal nanoparticles' surfaces. Nanotechnology. 2007;18:105101.

[3] Oberdörster G, Oberdörster E, Oberdörster J. Nanotoxicology: an emerging discipline evolving from studies of ultrafine particles. Environ Health Perspect. 2005;113:823–39.

[4] Kumar SV, Rajeshkumar S. Plant-based synthesis of nanoparticles and their impact. Nanomaterials in plants, algae, and microorganisms. Concepts Controversies. 2018;3: 33–57.

[5] Kumar P, Santhakumar K, Tatsugi J, Shin P-K, Ochiai S. Comparison of properties of polymer organic solar cells prepared using highly conductive modified PEDOT: PSS films by spin-and spray-coating methods. Jpn J Appl Phys. 2013;53:01AB8.

[6] Mittal AK, Chisti Y, Banerjee UC. Synthesis of metallic nanoparticles using plant extracts. Biotechnol Adv. 2013;31:346–56.

[7] Abdel-Hameed E-SS. Total phenolic contents and free radical scavenging activity of certain Egyptian Ficus species leaf samples. Food Chem. 2009;114:1271–7.

[8] Mahendra C, Murali M, Manasa G, Ponnamma P, Abhilash M, Lakshmeesha T, et al. Antibacterial and antimitotic potential of bio-fabricated zinc oxide nanoparticles of *Cochlospermum religiosum* (L.). Microb Pathogenesis. 2017;110: 620–9.

[9] Sukri SNAM, Shameli K, Wong MM-T, Teow S-Y, Chew J, Ismail NA. Cytotoxicity and antibacterial activities of plant-mediated synthesized zinc oxide (ZnO) nanoparticles using Punica granatum (pomegranate) fruit peels extract. J Mol Structure. 2019;1189:57–65.

[10] Bokhari M, Edmondson J. Acantholimon boiss. Flora Turk East Aegean Isl. 1982;7:478–502.

[11] Lashgari AP, Delazar A, Afshar FH, Parsa D. Contact toxicity and chemical composition of essential oil of Acantholimon scorpius. Pharm Sci. 2016;22:138.

[12] Gazor R, Asgari M, Pasdaran A, Mohammadghasemi F, Nasiri E, Roushan ZA. Evaluation of hepatoprotective effect of acantholimon gilliati eerial part methanolic extract. Iran J Pharm Res: IJPR. 2017;16:135.

[13] Nasiri E, Naserirad S, Pasdaran LA, Gazor R, Mohammadghasemi F, Atrkar RZ. Hepatoprotective effect of Acantholimon bracteatum (Girard) Boiss. on formaldehyde-induced liver injury in adult male mice. Res J Pharm. 2016;3:55–61.

[14] Gunaherath GKB, Gunatilaka AL, Sultanbawa MUS, Balasubramaniam S. 1, 2 (3)-Tetrahydro-3,3′-biplumbagin: A naphthalenone and other constituents from *Plumbago zeylanica*. Phytochemistry. 1983;22:1245–7.

[15] Pavela R. Efficacy of naphthoquinones as insecticides against the house fly, *Musca domestica* L. Ind Crop Products. 2013;43:745–50.

[16] Nabi S, Baloch NU, Bashir S, Rabbani T, Al-Kahraman YM. *In vitro* antimicrobial, antitumor and cytotoxic activities and their phytochemical analysis of methanolic extract and its fractions of acantholimon longiscapum leaves. Int J Phytoph. 2013;4:179–83.

[17] Soltanian S, Sheikhbahaei M, Mansour M, Behjat KK. Evaluation of anticancer, antioxidant and antibacterial properties of methanol extract of three Acantholimon Boiss. species. Avicenna J Phytomed. 2020;10:641–52.

[18] Soltanian S, Sheikhbahaei M, Mohamadi N. Cytotoxicity evaluation of methanol extracts of some medicinal plants on P19 embryonal carcinoma cells. J Appl Pharm Sci. 2017;7:142–9.

[19] Soltanian S, Mohamadi N, Rajaei P, Khodami M, Mohammadi M. Phytochemical composition, and cytotoxic, antioxidant, and antibacterial activity of the essential oil and methanol extract of Semenovia suffruticosa. Avicenna J Phytomed. 2019;9:143.

[20] Singh N, Haque FZ. Synthesis of zinc oxide nanoparticles with different pH by aqueous solution growth technique. Optik. 2016;127:174–7.

[21] Soltanian S, Sheikhbahaei M, Ziasistani M. Phytol down-regulates expression of some cancer stem cell markers and decreases side population proportion in human embryonic carcinoma NCCIT cells. Nutr Cancer. 2020;1–14.

[22] Marimoutou M, Le Sage F, Smadja J, d'Hellencourt CL, Gonthier M-P, Robert-Da, et al. Antioxidant polyphenol-rich extracts from the medicinal plants Antirhea borbonica, *Doratoxylon apetalum* and *Gouania mauritiana* protect 3T3-L1 preadipocytes against H_2O_2, TNFα and LPS inflammatory mediators by regulating the expression of superoxide dismutase and NF-κB genes. J Inflamm. 2015;12:10.

[23] Cui D, Liang T, Sun L, Meng L, Yang C, Wang L, et al. Green synthesis of selenium nanoparticles with extract of hawthorn fruit induced HepG2 cells apoptosis. Pharm Biol. 2018;56:528–34.

[24] Al-Sheddi ES, Farshori NN, Al-Oqail MM, Al-Massarani SM, Saquib Q, Wahab R, et al. Anticancer potential of green synthesized silver nanoparticles using extract of Nepeta deflersiana against human cervical cancer cells (HeLA). Bioinorg Chem Appl. 2018;2:1–12.
[25] Soltanian S, Riahirad H, Pabarja A, Karimzadeh MR, Saeidi K. Kaempferol and docetaxel diminish side population and downregulate some cancer stem cell markers in breast cancer cell line MCF-7. Biocell. 2017;41:33.
[26] Soltanian S, Riahirad H, Pabarja A, Jafari E, Khandani BK. Effect of Cinnamic acid and FOLFOX in diminishing side population and downregulating cancer stem cell markers in colon cancer cell line HT-29. DARU. J Pharm Sci. 2018;26:19–29.
[27] Baharara J, Namvar F, Ramezani T, Mousavi M, Mohamad R. Silver nanoparticles biosynthesized using Achillea biebersteinii flower extract: apoptosis induction in MCF-7 cells via caspase activation and regulation of Bax and Bcl-2 gene expression. Molecules. 2015;20:2693–706.
[28] Salehi S, Shandiz SAS, Ghanbar F, Darvish MR, Ardestani MS, Mirzaie A, et al. Phytosynthesis of silver nanoparticles using Artemisia marschalliana Sprengel aerial part extract and assessment of their antioxidant, anticancer, and antibacterial properties. Int J Nanomed. 2016;11:1835.
[29] Shaik MR, Khan M, Kuniyil M, Al-Warthan A, Alkhathlan HZ, Siddiqui MRH, et al. Plant-extract-assisted green synthesis of silver nanoparticles using Origanum vulgare L. extract and their microbicidal activities. Sustainability. 2018;10:913.
[30] Senthilkumar N, NandhaKumar E, Priya P, Soni D, Vimalan M. Potheher IV. Synthesis, anti-bacterial, antiarthritic, anti-oxidant and in-vitro cytotoxicity activities of ZnO nanoparticles using leaf extract of Tectona Grandis (L.). N J Chem. 2017;41:10347–56.
[31] Yuvakkumar R, Suresh J, Saravanakumar B, Nathanael AJ, Hong SI, Rajendran V. Rambutan peels promoted biomimetic synthesis of bioinspired zinc oxide nanochains for biomedical applications. Spectrochimica Acta Part A: Mol Biomol Spectrosc. 2015;137:250–8.
[32] Stockert JC, Horobin RW, Colombo LL, Blázquez-Castro A. Tetrazolium salts and formazan products in cell biology: viability assessment, fluorescence imaging, and labeling perspectives. Acta Histochemica. 2018;120:159–67.
[33] Van Engeland M, Nieland LJ, Ramaekers FC, Schutte B, Reutelingsperger CP. Annexin V-affinity assay: a review on an apoptosis detection system based on phosphatidylserine exposure. Cytometry: J Int Soc Anal Cytology. 1998;31:1–9.
[34] Zimmermann M, Meyer N. Annexin V/7-AAD staining in keratinocytes. Mammalian Cell Viability. 2011;3:57–63.
[35] Puišo J, Jonkuvienė D, Mačionienė I, Šalomskienė J, Jasutienė I, Kondrotas R. Biosynthesis of silver nanoparticles using lingonberry and cranberry juices and their antimicrobial activity. Colloids Surf B: Biointerfaces. 2014;121:214–21.
[36] Chouhan HS, Sharma A. Int J Green Herb Chem Int J. 2014;3:425–33.
[37] Gnanasangeetha D, Thambavani DS. Biogenic production of zinc oxide nanoparticles using Acalypha indica. J Chem, Biol Phys Sci (JCBPS). 2013;4:238.
[38] Manokari M, Shekhawat MS. Biogenesis of zinc oxide nanoparticles using aqueous extracts of hemidesmusindicus (l.) r. Br Int J Res Stud Microbiol Biotechnol. 2015;1:20–4.
[39] Umar H, Kavaz D, Rizaner N. Biosynthesis of zinc oxide nanoparticles using Albizia lebbeck stem bark, and evaluation of its antimicrobial, antioxidant, and cytotoxic activities on human breast cancer cell lines. Int J Nanomed. 2019;14:87.
[40] Abbasi BH, Shah M, Hashmi SS, Nazir M, Naz S, Ahmad W, et al. Green bio-assisted synthesis, characterization and biological evaluation of biocompatible ZnO NPs synthesized from different tissues of milk thistle (*Silybum marianum*). Nanomaterials. 2019;9:1171.
[41] Happy A, Soumya M, Kumar SV, Rajeshkumar S, Sheba RD, Lakshmi T, et al. Phyto-assisted synthesis of zinc oxide nanoparticles using Cassia alata and its antibacterial activity against Escherichia coli. Biochem Biophys Rep. 2019;17:208–11.
[42] Sirelkhatim A, Mahmud S, Seeni A, Kaus NHM, Ann LC, Bakhori SKM, et al. Review on zinc oxide nanoparticles: antibacterial activity and toxicity mechanism. Nano-Micro Lett. 2015;7:219–42.
[43] Doğan SŞ, Kocabaş A. Green synthesis of ZnO nanoparticles with Veronica multifida and their antibiofilm activity. Hum & Exp Toxicol. 2019;39:319–27.
[44] Rauf MA, Oves M, Rehman FU, Khan AR, Husain N. Bougainvillea flower extract mediated zinc oxide's nanomaterials for antimicrobial and anticancer activity. Biomed Pharmacother. 2019;116:108983.
[45] Ghanbar F, Mirzaie A, Ashrafi F, Noorbazargan H, Jalali MD, Salehi S, et al. Antioxidant, antibacterial and anticancer properties of phyto-synthesised Artemisia quttensis Podlech extract mediated AgNPs. IET Nanobiotechnol. 2016;11:485–92.
[46] Mohanta YK, Panda SK, Jayabalan R, Sharma N, Bastia AK, Mohanta TK. Antimicrobial, antioxidant and cytotoxic activity of silver nanoparticles synthesized by leaf extract of Erythrina suberosa (Roxb.). Front Mol Biosci. 2017;4:14.
[47] Prashanth G, Prashanth P, Bora U, Gadewar M, Nagabhushana B, Ananda S, et al. *In vitro* antibacterial and cytotoxicity studies of ZnO nanopowders prepared by combustion assisted facile green synthesis. Karbala Int J Mod Sci. 2015;1:67–77.
[48] Wang C, Hu X, Gao Y, Ji Y. ZnO nanoparticles treatment induces apoptosis by increasing intracellular ROS levels in LTEP-a-2 cells. BioMed Res Int. 2015;5617:423287.
[49] Rosarin FS, Arulmozhi V, Nagarajan S, Mirunalini S. Antiproliferative effect of silver nanoparticles synthesized using amla on Hep2 cell line. Asian Pac J Tropical Med. 2013;6:1–10.
[50] Bai D-P, Zhang X-F, Zhang G-L, Huang Y-F, Gurunathan S. Zinc oxide nanoparticles induce apoptosis and autophagy in human ovarian cancer cells. Int J Nanomed. 2017;12:6521.
[51] Zare E, Pourseyedi S, Khatami M, Darezereshki E. Simple biosynthesis of zinc oxide nanoparticles using nature's source, and it's *in vitro* bio-activity. J Mol Structure. 2017;1146:96–103.
[52] Saliani M, Jalal R, Goharshadi EK. Mechanism of oxidative stress involved in the toxicity of ZnO nanoparticles against eukaryotic cells. Nanomed J. 2016;3:1–14.
[53] Tsujimoto Y. Role of Bcl-2 family proteins in apoptosis: apoptosomes or mitochondria? Genes Cell. 1998;3:697–707.

[54] Ahmadi Shadmehri A, Namvar F, Miri H, Yaghmaei P, Nakhaei Moghaddam M. Assessment of antioxidant and antibacterial activities of zinc oxide nanoparticles, graphene and graphene decorated by zinc oxide nanoparticles. Int J Nano Dimens. 2019;10:350–8.
[55] Yuan Y-G, Wang Y-H, Xing H-H, Gurunathan S. Quercetin-mediated synthesis of graphene oxide–silver nanoparticle nanocomposites: a suitable alternative nanotherapy for neuroblastoma. Int J Nanomed. 2017;12:5819.
[56] Ogunyemi SO, Abdallah Y, Zhang M, Fouad H, Hong X, Ibrahim E, et al. Green synthesis of zinc oxide nanoparticles using different plant extracts and their antibacterial activity against Xanthomonas oryzae pv. oryzae. Artif Cells, Nanomed, Biotechnol. 2019;47:341–52.
[57] Ovais M, Khalil AT, Islam NU, Ahmad I, Ayaz M, Saravanan M, et al. Role of plant phytochemicals and microbial enzymes in biosynthesis of metallic nanoparticles. Appl Microbiol Biotechnol. 2018;102:6799–814.
[58] Ovais M, Khalil AT, Ayaz M, Ahmad I, Nethi SK, Mukherjee S. Biosynthesis of metal nanoparticles via microbial enzymes: a mechanistic approach. Int J Mol Sci. 2018;19:4100.